Loading of MOF-5 with Cu and ZnO Nanoparticles by Gas-Phase Infiltration with Organometallic Precursors: Properties of Cu/ZnO@MOF-5 as Catalyst for Methanol Synthesis

Maike Müller,[†] Stephan Hermes,[†] Kevin Kähler,[‡] Maurits W. E. van den Berg,[‡] Martin Muhler,[‡] and Roland A. Fischer*,[†]

Chair of Inorganic Chemistry II, Organometallics and Materials Chemistry and Department of Industrial Chemistry, Ruhr-University Bochum, D-44870 Bochum, Germany

Received November 23, 2007. Revised Manuscript Received February 27, 2008

The loading of $[Zn_4O(bdc)_3]$ (MOF-5; bdc = 1,4-benzenedicarbocylate) with nanocrystalline Cu and ZnO species was achieved in a two-step process. First, the solvent-free gas-phase adsorption of the volatile precursors [CpCuL] (L = PMe_3, CN^tBu) and $ZnEt_2$ leads to the isolable inclusion compounds precursor@MOF-5. These intermediates were then converted into Cu@MOF-5 and ZnO@MOF-5 by hydrogenolysis or photoassisted thermolysis at 200−220 °C in the case of Cu and hydrolysis or dry oxidation at 25 °C followed by annealing 250 °C in the case of ZnO. ^{17}O labeling studies using $H_2{}^{17}O$ (30%) revealed that neither the bdc linkers nor the central oxide ion of the Zn_4O unit exchange oxygen atoms/ions with the imbedded ZnO species. The obtained material Cu@MOF-5 (11 wt % Cu), exhibiting an equivalent Langmuir surface of 1100 $m^2 \cdot g^{-1}$, was further characterized by powder X-ray diffraction (PXRD), X-ray absorption spectroscopy (XAS), and transmission electron microscopy (TEM). The Cu nanoparticles are homogeneously distributed over the MOF-5 microcrystals, occupying only about 1% of the cavities. Their size distribution appears to be polydisperse with a majority around 1 nm in size (by EXAFS) together with a minority of larger particles up to 3 nm (PXRD). Cu@MOF-5 was reversibly surface oxidized/reduced by N_2O/H_2 treatment, resulting in a (Cu_2O/Cu)@MOF-5 material as revealed by PXRD and XAS. Depending on the preparation conditions of the ZnO@MOF-5 materials a variation of the ZnO loading from 10 to 35 wt % was achieved. PXRD, TEM, UV−vis, and ^{17}O-MAS NMR spectroscopy gave evidence for a largely intact MOF-5 matrix with imbedded ZnO nanoparticles <4 nm being in the quantum size regime. Doubly-loaded (Cu/ZnO)@MOF-5 samples were prepared by gas-phase loading of ZnO@MOF-5 with [CpCuL] followed by thermally activated hydrogenolysis. The initial catalytic productivity in methanol synthesis from a $CO/CO_2/H_2$ gas mixture at 1 atm and 220 °C peaked at about 60% of an industrial reference catalyst. This result is particular surprising because of the comparably low Cu loading (1.4 wt %) and small Cu specific surface area <1 $m^2 \cdot g^{-1}$, thus suggesting a superior interfacial contact between the Cu and ZnO nanophases. However, the materials (Cu/ZnO)@MOF-5 were unstable under catalytic conditions over several hoours, the metal organic framework collapsed, and the final catalytic activities were poor.

Introduction

Porous coordination polymers in general and the so-called metal−organic open frameworks (MOFs) in particular represent an interesting class of inorganic/organic hybrid materials with zeolite-like structures and properties, a chemistry which was pioneered, namely, by S. Kitagawa, O. M. Yaghi, M. O'Keeffe, and G. Ferey.[1–4] MOFs are based on the coordination chemistry of metal ions M^+ with bi-, tri-, or even tetrafunctional organic carboxylates leading to networks of perfect translational symmetry and exhibiting molecularly defined cavities for the adsorption of guest molecules, imbedding of nanoclusters, or more generally for anchoring of functional species. For example, so-called MOF-5 (IRMOF-1), i.e., $[Zn_4O(bdc)_3]$ (bdc = benzene-1,4-dicarboxylate), MOF-177, i.e., $[Zn_4O(btb)_2]$ (btb = benzene-1,3,5-tribenzoate), and MIL-101, i.e., $[Cr_3F(H_2O)_2O(btc)_3]$ (btc = benzene-1,3,5-tricarboxylate) exhibit extraordinarily high H_2-absorption capacities at 77 K. This property corresponds to equivalent Langmuir surface areas and pore volumes of 3200 $m^2 \cdot g^{-1}$ and 1.03 $cm^3 \cdot g^{-1}$ for MOF-5, 4500 $m^2 \cdot g^{-1}$ and 1.59 $cm^3 \cdot g^{-1}$ for MOF-177, or even 5900 $m^2 \cdot g^{-1}$ and 2.0 $cm^3 \cdot g^{-1}$ for MIL-101.[5–8] MOFs have

* To whom correspondence should be addressed. E-mail: roland.fischer@rub.de.
[†] Chair of Inorganic Chemistry II, Organometallics and Materials Chemistry.
[‡] Chair of Technical Chemistry.

(1) (a) Delgado-Friedrichs, O.; O'Keeffe, M.; Yaghi, O. M. *Phys. Chem. Chem. Phys.* **2007**, *9*, 1035. (b) Rowsell, J. L. C.; Yaghi, O. M. *Angew. Chem., Int. Ed.* **2005**, *44*, 4670. (c) Rowsell, J. L. C.; Yaghi, O. M. *Microporous Mesoporous Mater.* **2004**, *73*, 3.
(2) Ferey, G.; Mellot-Draznieks, C.; Serre, C.; Millange, F. *Acc. Chem. Res.* **2005**, *38*, 217.
(3) Kitagawa, S.; Kitaura, R.; Noro, S. *Angew. Chem., Int. Ed.* **2004**, *43*, 2334.
(4) (a) May, L. J.; Shimizu, G. K. H. Z. *Kristallografiya* **2005**, *220*, 364. (b) Rao, C. N. R.; Natarajan, S.; Vaidhyanathan, R. *Angew. Chem., Int. Ed.* **2004**, *43*, 1466. (c) Janiak, C. *Dalton Trans.* **2003**, *14*, 2781.
(5) Li, H.; Eddaoudi, M.; O'Keeffe, M.; Yaghi, O. M. *Nature* **1999**, *402*, 276.
(6) Rowsell, J. L. C.; Millward, A. R.; Park, K. S.; Yaghi, O. M. *J. Am. Chem. Soc.* **2004**, *126*, 5666.

10.1021/cm703339h CCC: $40.75
Published on Web 06/18/2008

attracted much recent interest as catalysts[9–11] and/or support materials for active metals or complexes in heterogeneous catalysts[12,13] as well as materials for gas storage[14] and gas separation.[15] For example, S. Kaskel et al. recently demonstrated the loading of MOF-5 with Pd by solution infiltration of [Pd(acac)$_2$] ("incipient wetness impregnation") and subsequent thermally activated hydrogenolysis of the imbedded precursor. The resulting material Pd@MOF-5 (1 wt % Pd) was tested for ethylbenzene hydrogenation and hydrogen storage.[13] An alternative loading technique is solvent-free gas-phase infiltration with organometallic precursors [ML$_n$] derived from MOCVD to yield inclusion compounds of the type [ML$_n$]$_m$@MOF as intermediates.[12,16] We used this concept to prepare supported catalysts Cu@MOF-5 (~10 wt % Cu) and communicated surprising activity in methanol synthesis from CO and H_2.[12] Copper alone exhibits almost no activity in methanol synthesis. Zinc oxide is the typical promoter for copper-based methanol catalysts, and the binary system Cu/ZnO prepared by conventional coprecipitation/calcination techniques represents a prototype of the so-called strong metal support interaction in heterogeneous catalysis.[17] The catalytic properties of Cu/ZnO imbedded into mesoporous silica matrices, i.e., (Cu/ZnO)MCM-41/48, suggest a superior interfacial contact between the Cu and the ZnO phase. The activity of these materials with respect to the accessible Cu surface area were higher as compared with reference samples of industrial catalysts.[18] Within this context we were interested in loading MOF-5 with both Cu *and* ZnO nanoparticles and derive a material of the type (Cu/ZnO)@MOF-5. The ZnO loading of inorganic matrices such as zeolites (e.g., H-ZSM-5) and periodic mesoporous silica materials (e.g., MCM-41/48, SBA-15) has been studied in this context previously[19] and was also motivated by the investigation of size-quantization effects of ZnO.[20] However, there has been no report in the literature of loading MOFs with metal oxide or compound semiconductor nanoparticles so far.

Experimental Section

General Techniques and Materials. All manipulations were carried out under inert conditions using Schlenk-line and glovebox techniques (Ar, H_2O, below 1 ppm). Solvents were purified, dried, and saturated with Ar using an automatic catalytic solvent purification system (MBraun, Garching). The employed MOCVD precursor [$(C_2H_5)_2$Zn] was purchased from Aldrich and used as received. The copper precursors [CpCuL] (L = PMe_3, CN^tBu) were prepared according to the literature.[21] The pure, desolvated (activated) MOF-5 material [$Zn_4O(bdc)_3$] was synthesized following the procedure published by Yaghi et al. with some modifications as described elsewhere.[22] The inclusion compounds [CpCuL]$_n$@MOF-5 (n = 1, 2) were derived and characterized as described in detail previously.[16] The samples of ^{17}O-labeled MOF-5 and ZnO were prepared and characterized as reference materials as described below.

^{17}O-Labeled MOF-5. ^{17}O-Labeled terephthalic acid was prepared as follows: A sample of 2 g of terephthalic acid was dissolved in 10 mL of DMSO. A volume of 1 mL of ^{17}O-enriched water (30%), previously saturated with gaseous HCl, was quickly added via a syringe to the DMSO solution. The resulting suspension was heated to reflux for a period of 24 h. The ^{17}O-labeled terephthalic acid was quantitatively precipitated at 0 °C by addition of 5 mL of ordinary deionized water, collected by suction filtration through a glass frit, and dried in vacuum subsequently (yield 1.95 g, 95%). The spectroscopic data are listed at the end of this paragraph. For the preparation of doubly-labeled ^{17}O-MOF-5^{ab} a sample of 0.665 g of ^{17}O-enriched terephthalic acid (8.3%) together with a sample of 3.14 g of $Zn(NO_3)_2 \cdot 4\ H_2O$ was dissolved in 100 mL of pure and dry DEF. A volume of 0.3 mL of ^{17}O-enriched water (30%) was added, and the mixture was heated to 105 °C and kept at this temperature for 24 h. After cooling to room temperature, the deposited colorless, cubic crystals of several millimeters in size were collected and worked up to remove the adsorbed solvent as described in the literature for MOF-5.[22] The analytical data matched reference data of authentic compounds and literature data as well (see below). Samples of selectively single-site-labeled ^{17}O-MOF-5^a and ^{17}O-MOF-5^b were synthesized following the above procedure but without the use of ^{17}O-enriched water in the case of MOF-5^a and using ordinary terephthalic acid in combination with ^{17}O-enriched water in the case of MOF-5^b, respectively. The obtained analytical data matched the data given for MOF-5^{ab} below and are thus not documented here. However, in the case of MOF-5^a the ^{17}O NMR resonance of the Zn_4O unit at −50 ppm was absent while

(7) Chae, H. K.; Siberio-Perez, D. Y.; Kim, J.; Go, Y. M.; Eddaoudi, A. J.; Matzger, M.; O'Keeffe, M.; Yaghi, O. M. *Nature* **2004**, *427*, 523.
(8) Ferey, G.; Mellot-Drazniek, C.; Serre, C.; Millange, F.; Dutour, J.; Surble, S.; Margiolaki, I. *Science* **2005**, *309*, 2040.
(9) (a) Kaskel, S. *Nachr. Chem.* **2005**, *53*, 394. (b) Schlichte, K.; Kratzke, T.; Kaskel, S. *Microporous Mesoporous Mater.* **2004**, *73*, 81.
(10) Budd, P. M.; Ghanem, B.; Msayib, K.; McKeown, N. B.; Tattershall, C. *J. Mater. Chem.* **2003**, *13*, 2721.
(11) Moon, H. R.; Kim, J. H.; Suh, M. P. *Angew. Chem., Int. Ed.* **2005**, *44*, 1261.
(12) Hermes, S.; Schröter, M.-K.; Schmid, R.; Khodeir, L.; Muhler, M.; Tissler, A.; Fischer, R. W.; Fischer, R. A. *Angew. Chem., Int. Ed.* **2005**, *44*, 6237.
(13) Sabo, M.; Henschel, A.; Froede, H.; Klemm, E.; Kaskel, S. *J. Mater. Chem.* **2007**, *17*, 3827.
(14) Rosi, N. L.; Eckert, J.; Eddaoudi, M.; Vodak, D. T.; Kim, J.; O'Keeffe, M.; Yaghi, O. M. *Nature* **2003**, *423*, 1127.
(15) Chen, B.; Liang, C.; Yang, J.; Contreras, D. S.; Damacio, S.; Clancy, Y. L.; Lobkovsky, E. B.; Yaghi, O. M.; Dai, S. *Angew. Chem., Int. Ed.* **2006**, *45*, 1390.
(16) (a) Hermes, S.; Schröder, F.; Amirjalayer, S.; Schmid, R.; Fischer, R. A. *J. Mater. Chem.* **2006**, *16*, 2464. (b) Hermes, S.; Schröder, F.; Chelmowski, R.; Wöll, C.; Fischer, R. A. *J. Am. Chem. Soc.* **2005**, *127*, 13744.
(17) (a) Hansen, P. L.; Wagner, J. B.; Helveg, S.; Rostrup-Nielsen, J. R.; Clausen, B. S.; Topsoe, H. *Science* **2002**, *295*, 2053. (b) Kasatkin, I.; Kurr, P.; Kniep, B.; Trunschke, A.; Schlögl, R. *Angew. Chem., Int. Ed.* **2007**, *46*, 7324.
(18) (a) van den Berg, M. W. E.; Polarz, S.; Tkachenko, O. P.; Klementiev, K. V.; Bandyopadhyay, M.; Khodeir, L.; Gies, H.; Muhler, M.; Grunert, W. *J. Catal.* **2006**, *241*, 446. (b) Becker, R.; Parala, H.; Hipler, F.; Tkachenko, O. P.; Klementiev, K.; Grunert, W.; Wilmer, H.; Hinrichsen, O.; Muhler, M.; Birkner, A.; Woell, C.; Schafer, S.; Fischer, R. A. *Angew. Chem., Int. Ed.* **2004**, *43*, 2839.
(19) (a) Schröder, F.; Hermes, S.; Parala, H.; Hikov, T.; Muhler, M.; Fischer, R. A. *J. Mater. Chem.* **2006**, *16*, 3565. (b) Polarz, S.; Neues, F.; van den Berg, M. W. E.; Grünert, W.; Khodeir, L. *J. Am. Chem. Soc.* **2005**, *127*, 12028.
(20) (a) Chen, H. G.; Shi, J. L.; Chen, H. R.; Yan, J. N.; Li, Y. S.; Hua, Z. L.; Yang, Y.; Yan, D. S. *Opt. Mater.* **2004**, *25*, 79. (b) Dapurka, S. E.; Badamali, S. K.; Selvam, P. *Catal. Today* **2001**, *68*, 63. (c) Zhang, W.-H.; Shi, J.-L.; Wang, L.-Z.; Yan, D.-S. *Chem. Mater.* **2000**, *12*, 1408. (d) Haase, M.; Weller, H.; Henglein, A. *J. Phys. Chem.* **1988**, *92*, 482. (e) Chinchen, G. C.; Hay, C. M.; Vandervell, H. D.; Waugh, K. C. *J. Catal.* **1987**, *103*, 79–86.
(21) (a) Werner, H.; Otto, H.; Ngo-Khac, T.; Burschka, C. *J. Organomet. Chem.* **1984**, *262*, 123. (b) Ito, Y.; Saegusa, T.; Tomita, S. *J. Am. Chem. Soc.* **1971**, *93*, 5656.
(22) Yaghi, O. M.; Eddaoudi, M.; Li, H.; Kim, J.; Rosi, N. Patent WO 02/088148 A1, 2002.

Table 1. Elemental Analysis Data and Langmuir Surface Area of Representative Samples of [CpCuL]@MOF-5, Cu@MOF-5, ZnO@MOF-5, and (Cu/ZnO)@MOF-5 Prepared by Hydrogenation or Hydrolysis/Annealing of the Intermediates Precursor@MOF-5 under Different Conditions

	elemental analysis, measd/calcd[a] [wt %]				
sample	Cu	Zn	C	H	Langmuir surface area [m^2/g]
MOF-5		33.8/34.0	37.2/37.4	1.6/1.6	3200
$[CpCu(PMe_3)]_2$@MOF-5 (**1**)	10.7/10.8	22.0/22.2	40.4/40.7	3.4/3.4	*b*
Cu@MOF-5, from **1**, photoassisted	11.0/14.2	27.9/29.2	34.6/32.1	2.0/1.3	1070
Cu@MOF-5, from **1**, pyrolysis	11.2/14.2	28.0/29.2	34.2/32.1	1.9/1.3	1000
$[CpCu(CN^tBu)]_1$@MOF-5 (**2**)	6.5/4.3	22.9/21.9	41.6/39.6	2.6/3.0	*b*
Cu@MOF-5, from **2**, pyrolysis	6.0/7.6	31.3/31.4	34.7/35.6	2.1/1.5	1100
$[ZnO]_1$@MOF-5, method B		35.5/38.4	33.9/31.9	1.8/1.4	*b*
$[ZnO]_2$@MOF-5, method A, 248 K		42.1/42.0	30.2/30.9	1.4/1.3	*b*
$[ZnO]_2$@MOF-5, method A, 278 K		41.9/42.0	31.2/30.9	1.4/1.3	*b*
$[ZnO]_2$@MOF-5, method A, 298 K		41.8/42.0	31.1/30.9	1.3/1.3	900
$[ZnO]_5$@MOF-5, method B		47.6/50.0	24.3/24.5	2.1/1.0	1750
Cu/ZnO@MOF-5, from A	1.4/-	41.5/-	30.5/−	1.4/−	820
Cu/ZnO@MOF-5, from B	7.9/-	43.0/-	24.5/−	1.8/−	*b*

[a] The calculated values refer to postulated integer numbers of formula units of [CpCuL], Cu, $ZnEt_2$, and ZnO per formula unit of MOF-5. The deviations of the measured and calculated values are explained by an inhomogeneous or not perfectly ordered distribution of the precursor molecules over the microcrystals of the sample. In addition, some desorption during the decomposition of the precursors has to be taken into account. [b] Langmuir surface area has not been determined.

for MOF-5[b] the ^{17}O NMR resonance for the carboxylic groups of the terephthalic acid at 202 ppm was absent.

Analytical Data for ^{17}O-Labeled Terephthalic Acid. ^1H-MAS NMR (δ_H/ppm): 8.1 [$C_6\mathbf{H_4}$]. ^{17}O-MAS NMR (δ_O/ppm): 189.9; 151.3 [**COO**]. FTIR (KBr), ν_{max} [cm^{-1}]: 3105 w, 3067 w, 2964 vw, 2929 vw, 2648 w, 2512 w, 1675 s, 1565 m, 1507 m, 1426 s, 1407 m, 1388 m, 1280 s, 1133 w, 1111 m, 1019 w, 934 m, 880 m, 778 m, 730 s, 560 w, 521 m, 450 vw. EI-MS (*m*/*z*): 168, 167, 166 (M^+, characteristic isotope pattern), 150, 149 (M − OH), 121 (M − COOH), 104 (M − COOH − OH), 76 (C_6H_4), 74, 73, 65, 51, 50, 45 (COOH), 39. ^{17}O Enrichment of 8.3%, calculated according to the formula $0.25\ I_{167}\cdot(I_{166}+I_{167})^{-1}$.

Analytical Data for ^{17}O-MOF-5[ab]. Anal. Calcd for $[Zn_4O[C_8H_4O_4]_3]$: Zn, 34.0; C, 37.4; H, 1.6. Found: Zn, 34.2; C, 38.1; H, 1.7%. FTIR (KBr), ν_{max} [cm^{-1}]: 1569 s, 1509 m, 1391 s, 1262 w, 1176 vw, 1154 w, 1101 w, 1018 m, 882 w, 819 w, 747 m, 521 m. PXRD capillary mode 2θ (rel. int. %): 11.4 (12.3); 13.7 (100); 15.0 (18.6); 15.4 (69.3); 16.9 (5.4); 17.9 (14.1); 19.6 (10.7); 20.4 (35.2); 20.7 (11.3); 22.6 (27.3); 22.8 (8.4); 24.7 (17.9); 25.9 (7.3); 26.6 (37.2); 28.5 (11.4); 29.4 (4.5); 30.0 (21.7); 31.6 (23.6); 33.2 (7.0); 34.6 (18.4); 35.6 (6.2); 36.0 (10.2); 37.4 (8.9); 38.8 (2.6); 40.0 (8.9); 41.4 (4.6); 42.1 (8.1); 42.6 (16.3); 43.3 (8.3); 43.6 (4.6); 44.5 (3.8); 45.0 (7.6); 45.6 (1.9). ^1H-MAS NMR (δ_H/ppm): 7.99 [$C_6\mathbf{H_4}$]. ^{13}C-MAS NMR (δ_C/ppm): 175.9 [**C**OO], 137.2 [**C**(COO)], 130.9 [$\mathbf{C_6}H_4$]. ^{17}O-MAS NMR (δ_O/ppm): 202.0 [C**OO**], −50.0 [$Zn_4\mathbf{O}$] (see Figure 8). N_2 gas adsorption studies revealed a type I isotherm leading to an equivalent Langmuir surface area of 3300 $m^2\cdot g^{-1}$.

^{17}O-Labeled ZnO. A vial was loaded with 1 mL of pure liquid $ZnEt_2$ and sealed with a polymer lid, which was perforated as described above, and finally placed in a Schlenk tube. Outside the dry box and using a Schlenk line (Ar), a sample of 1 mL of ^{17}O-enriched water was carefully placed at the bottom of the Schlenk tube without touching the lid of the vial using a syringe with a long needle. After sealing, the tube was left for 24 h at 25 °C. To ensure complete hydrolysis, most of the ^{17}O-enriched water at the bottom of the Schlenk tube was finally added to the prehydrolyzed $ZnEt_2$ in the vial by injection through the lid, again using a syringe. The deposited white powder was collected by decantation, dried in dynamic vacuo at 25 °C, and finally annealed at 250 °C (±5 °C) for 6 h. The analytical data matched values given in the literature. ^{17}O-MAS NMR (δ_O/ppm): −17.6 ppm.[23] PXRD capillary mode 2θ (rel. int. %, [*hkl*] assignment for hexagonal ZnO phase): 31.76 (67.1, [100]); 34.41 (43.2, [002]); 36.25 (100, [101]); 47.54 (17.7, [102]); 56.61 (30.9, [110]).

Cu- and ZnO-Loaded MOF-5: Sample Preparation. *Cu@MOF-5.* The loading of MOF-5 with Cu nanoparticles was performed by gas-phase infiltration of 100−250 mg of MOF-5 with excess $[CpCu(PMe_3)]$ or $[CpCu(CN^tBu)]$ following the detailed description given in the literature.[16] Samples (100 mg) of the resulting inclusion compounds $[CpCuPMe_3]_2$@MOF-5 (**1**) and $[CpCu(CN^tBu)]$@MOF-5 (**2**) were placed in a sealed quartz glass tube and photolyzed under argon (1 atm) using a mercury UV lamp (500 W, Normag, TQ 718) at 90−100 °C for 2 h with repeated shaking and rotation of the tube in order to ensure homogeneous irradiation. Alternatively, samples of **1** and **2** were treated with hydrogen (100%, 1 $sccm\cdot s^{-1}$) at 220 °C for 5 h. After photolysis/hydrogenolysis the volatile byproducts were desorbed at 120 °C in dynamic vacuo (10^{-2} mbar) over 12 h. The obtained red-brown-colored samples Cu@MOF-5 were stored under Ar. The elemental compositions were determined by AAS (Cu, Zn), and combustion analysis (C, H) data are compiled in Table 1. The N_2 gas adsorption studies revealed type I isotherms (Langmuir model). Values of 1065−1090 $m^2\cdot g^{-1}$ were extracted for the specific surface area. ^{13}C-MAS NMR and FTIR data of (i) Cu@MOF-5 derived from **1**. ^{13}C-MAS NMR (δ_C, ppm): 175.9 [COO], 140.0 [C(COO)], 132.2 [(C_6H_4)], 17.7 [$P(CH_3)_3$]. FTIR (KBr), ν_{max} [cm^{-1}]: 3076 w, 2970 w, 2905 w, 1712 m, 1604 s, 1503 m, 1382 s, 1290 m, 1145 s, 1018 w, 947 s, 860 w, 823 w, 749 s, 674 w, 524 m. (ii) Data of Cu@MOF-5 derived from **2**. ^{13}C-MAS NMR (δ_C, ppm): 175.9 [COO], 140.0 [C(COO)], 132.2 [(C_6H_4)]. FTIR (KBr) ν_{max} [cm^{-1}]: 2962 w, 1572 s, 1508 m, 1396 s 1264 m, 1154 m, 1106 w, 1018 m, 872 w, 828 w, 812 w, 748 s, 530 m. The PXRD, TEM, and XAS data of the materials are shown in Figures 1–3 and discussed in the main text.

(Cu_2O/Cu)@MOF-5. Samples of 200 mg of Cu@MOF-5 contained in glass vials were placed in a glass tube and treated with N_2O gas (0.5%, diluted in N_2, 1 $sccm\cdot s^{-1}$, ambient pressure) at various temperatures of 25, 170, and 220 °C for 2 h. The reduction back to Cu@MOF-5 was performed using pure hydrogen gas at 220 °C for 2 h. The oxidation/reduction cycles are accompanied by a color change from red-brown to black-green and back to red-brown. The samples (Cu_2O/Cu)@MOF-5 and Cu@MOF-5 were then stored under Ar for analytical characterization. The analytical data (PXRD, TEM) of the obtained Cu@MOF-5 after reduction were identical to the starting material and are not listed here. The

(23) Turner, G. L.; Chung, S. E.; Oldfield, E. *J. Magn. Reson.* **1985**, *64*, 316.

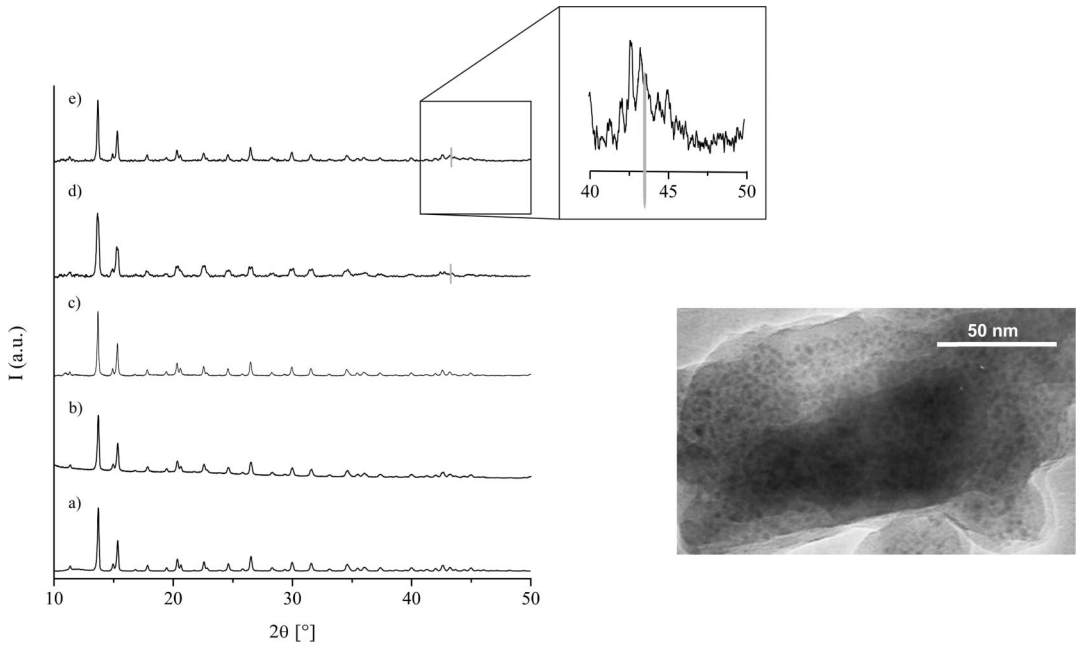

Figure 1. Powder X-ray diffraction patterns of (a) pure, activated MOF-5, (b) $[CpCu(PMe_3)]_2$@MOF-5, (c) [CpCu(CN^tBu)]@MOF-5, (d) Cu@MOF-5 (derived by treatment of **1** with 1 sccm H_2 at 220 °C for 5 h), (e) Cu@MOF-5 (derived by treatment of **2** with 1 sccm H_2 at 220 °C K for 5 h); enlargement of the region between 40° and 50° 2θ is shown as the insert (marked line indicates the Cu(111) reflection, JPDS No. 00-004-0836). TEM image of Cu@MOF-5 (derived by treatment of **1** with 1 sccm H_2 at 220 °C for 5 h).

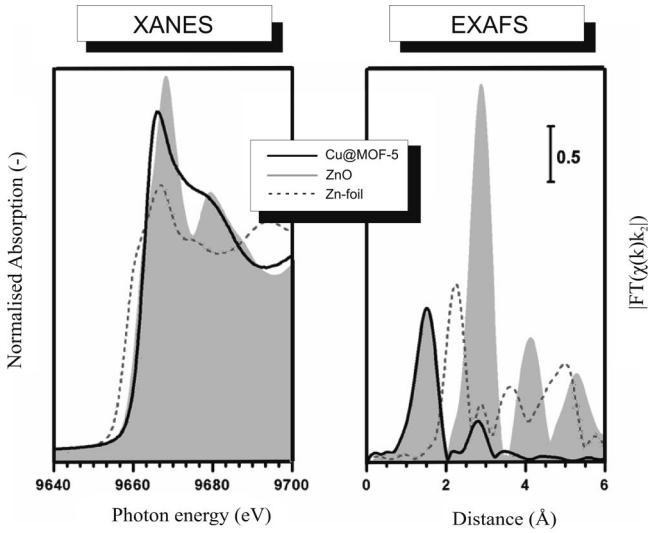

Figure 2. XANES (left) and EXAFS (right) at the Zn Kα edge of Cu@MOF-5 derived from **1** compared to ZnO and Zn foil.

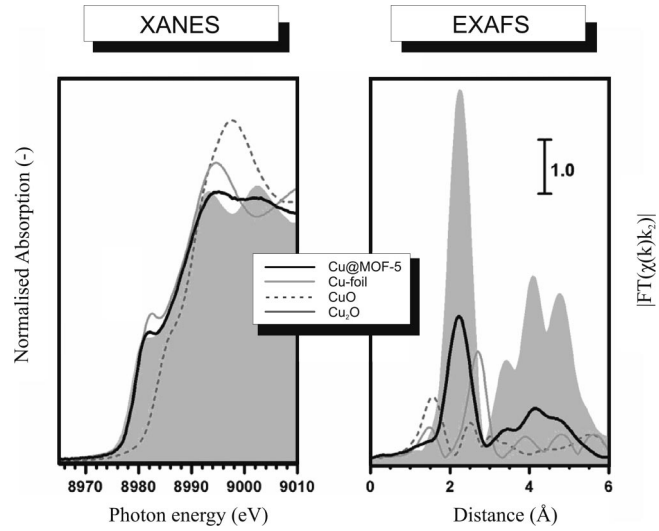

Figure 3. XANES (left) and EXAFS (right) at the Cu Kα edge of Cu@MOF-5 derived from **1** compared to CuO, Cu_2O, and Cu foil.

PXRD of (Cu_2O/Cu)@MOF-5 and the XAS data are discussed in the main text.

ZnO@MOF-5. The loading of MOF-5 with $ZnEt_2$ follows a procedure reported previously with some modifications.[16] In a typical experiment, a 100 mg sample of the activated (empty) MOF-5 material was placed into a vial placed in a sealed Schlenk tube together with a vial containing a certain amount of pure, liquid $ZnEt_2$ (i.e., = 0.03 mL, 0.29 mmol; 0.06 mL, 0.57 mmol; 0.09 mL, 0.86 mmol; 0.15 mL, 1.43 mmol). The Schlenk vessel was then cooled to −78 °C and evacuated to 10^{-3} mbar by connection to a vacuum line. The tube was sealed, allowed to warm up to 25 °C, and kept at this temperature for about 1 h to allow adsorption. No color change was visible. Then the Schlenk tube was transferred to a dry box (Ar; O_2 and H_2O below 1 ppm) and opened there for further manipulation. Because of the facile desorption of the weakly adsorbed $ZnEt_2$, the vials containing the inclusion compounds $[ZnEt_2]_n$@MOF-5 were sealed and stored in a refrigerator directly attached to the glovebox at −30 °C prior to further manipulation.

Method A. The vial with a sample of $[ZnEt_2]_n$@MOF-5 prepared from an adsorption experiment using 0.06 mL of $ZnEt_2$ (0.57 mmol) as described above was taken out of the Schlenk tube and sealed with a thin polymer lid (Parafilm). This lid was then perforated with a needle to allow for slow diffusion of moist air from the ambient air when placed outside the dry box. This smooth hydrolysis of the as-prepared $[ZnEt_2]_n$@MOF-5 material was conducted over 24 h at controlled temperatures of −30, 0, and 25 °C using three different samples by exposure of the vial to the ambient air outside the dry box. Representative samples of the three hydrolysis experiments were annealed at 250 °C (±5 °C) in dynamic vacuo (10^{-2} mbar) for 6 h and characterized by elemental analysis. The obtained data are compiled in Table 1 (above). Elemental analysis showed that about 2 equiv of ZnO were present per formula unit of MOF-5. Standard N_2 adsorption studies of a sample prepared

at 25 °C and annealed at 250 °C gave a value for the equivalent Langmuir surface area of 900 $m^2 \cdot g^{-1}$. ^{13}C-MAS NMR (δ_C, ppm): 175.9 [**C**OO], 140.0 [**C**(COO)], 132.2 [($\mathbf{C_6}H_4$)]. FTIR (KBr), ν_{max} [cm^{-1}]: 2961 vw, 2876 vw, 1565 s, 1509 m, 1397 s, 1160 w, 1103 w, 1053 w, 1019 m, 882 w, 829 w, 814 w, 748 m, 462 s.

Method B. The vials with samples $[ZnEt_2]_n$@MOF-5 prepared as described above were transferred into a glass tube under inert conditions (Ar, Schlenk line) and treated with a stream of diluted O_2 (4 vol. %, 1 $sccm \cdot s^{-1}$, ambient pressure) in Ar at 25 °C for 6 h. Subsequently, the samples were annealed at 250 °C in dynamic vacuo (10^{-3} mbar) for 24 h, and fractions were subjected to elemental analysis (Table 1) and further characterization. The NMR and FTIR data matched the characteristics of the ZnO@MOF-5 material prepared via method A and are not listed again here. Representative N_2 gas adsorption data for $[ZnO]_5$@MOF-5: N_2 1748 $m^2 \cdot g^{-1}$ (equivalent Langmuir surface).

ZnO@^{17}O-MOF-5^{ab} and Zn^{17}O@MOF-5. The two reference samples were prepared following the above-described method A for ZnO@MOF-5. Doubly-labeled ^{17}O-MOF-5^{ab} was loaded with $ZnEt_2$, which was converted into ZnO by hydrolysis and subsequent annealing, which resulted in a sample denoted as ZnO@^{17}O-MOF-5^{ab}. ^{17}O-enriched water (30%) was used for hydrolysis of the intermediate $[ZnEt_2]_2$@MOF-5 to finally yield a sample denoted as Zn^{17}O@MOF-5. The single-site-labeled samples ZnO@^{17}O-MOF-5^{a} and ZnO@^{17}O-MOF-5^{b} were synthesized accordingly. Similarly, the cross-labeled samples Zn^{17}O@^{17}O-MOF-5^{a} and Zn^{17}O@^{17}O-MOF-5^{b} were obtained. The analytical data (FTIR, PXRD, elemental analysis) of all these ^{17}O-labeled samples matched the data of the ZnO@MOF-5 reference samples above (and are thus not listed here), except for the representative ^{17}O NMR data (Figure 8), which are also discussed in the main text. ^{17}O-MAS NMR (δ_O/ppm): Zn^{17}O@MOF-5, −17.6 [ZnO]; ZnO@MOF-5^{ab}, 204 [COO], - 50 ppm [Zn_4O]; Zn^{17}O@MOF-5^{ab}, 204 [COO], −17.6 [ZnO], −50 ppm [Zn_4O].

(Cu/ZnO)@MOF-5. A sample of ZnO@MOF-5 (200 mg) prepared by hydrolysis according method A at 25 °C (see Table 1) was exposed to the vapor of [CpCu(PMe_3)] at 55 °C for 5 h similar to the previously described method for loading MOF-5 with volatile metal−organic precursors.[16] After cooling to 25 °C the loaded material ([CpCu(PMe_3)]/ZnO)@MOF-5 was transferred under inert conditions (Ar, glovebox) into a glass tube and treated with hydrogen gas (1 atm, 100%, 1 $sccm \cdot s^{-1}$, ambient pressure) at 220 °C for another 5 h, during which time the off-white color of the material turned slightly brownish. Desorption of volatile hydrocarbon decomposition products was performed at 90 °C in dynamic vacuo (10^{-2} mbar) for 12 h. The obtained material was stored under Ar. Elemental analysis is shown in Table 1. Standard N_2 adsorption studies of gave values for the equivalent Langmuir surface area of 820 $m^2 \cdot g^{-1}$. Figure 9 displays the PXRD pattern and TEM before and after catalysis.

Analytical Methods and Catalytic Testing. *FTIR, UV−vis, MAS NMR, Elemental Analysis, Nitrogen Absorption, PXRD, TEM, and XAS.* FTIR-spectra were measured as KBr disks with a Perkin-Elmer FTIR 1720 X spectrometer. UV−vis spectra were measured with a Perkin-Elmer Lambda 9 UV/vis/NIR spectrometer in reflection mode. Solid-state NMR spectra were measured with a Bruker DSX 400 MHz spectrometer under MAS conditions in 2.5 mm ZrO_2 rotors with a sample volume of 12 μL. The rotation frequency was 20 kHz. For the proton NMR measurements a ZG4PM pulse program was used. The carbon NMR measurements were carried out with the pulse program CP4C (cross polarization) and referenced to adamantine at 38.56 ppm. The ^{17}O NMR measurements were referenced to water at 0 ppm. For determination of the copper and zinc contents an AAS apparatus by Vario of type 6 (1998) was employed; C and H analyses were carried out using a Vario CHNSO EL (1998) instrument. Nitrogen adsorption experiments were carried out with a Quantachrome Autosorb-1 MP. The specific surface areas were calculated by fitting the measured type I isotherms to the Langmuir surface model in a pressure range of $p/p_0 = 0.1-0.3$ at $T = 77.36$ K. Powder XRD (PXRD) of the samples were recorded with a D8-Advance Bruker AXS diffractometer with Cu Kα radiation ($\lambda = 1.5418$ Å) in $\theta-2\theta$ geometry and with a position-sensitive detector. The experimental setup was in the capillary mode. For data accumulation, the samples were filled under inert gas (glovebox) into capillaries which were then sealed. Transmission electron microscopy (TEM) was done at a Hitachi H-8100 instrument equipped with a LaB_6 filament at 200 kV. EDX spectra were recorded with an Oxford-Link system (Si/Li crystal, ATW2 window). The samples were prepared in the glovebox (Au grid Plano 300 mesh) and transferred to the instrument under inert conditions (mobile high-vacuum chamber).

X-ray Absorption Spectra. The absorption edges of Zn at 9659 eV and Cu at 8979 eV were measured at the Hasylab E4 station (Hamburg, Germany). This beam line was equipped with a Si(111) double-crystal monochromator that was used to detune to 50% of the maximum intensity in order to exclude higher harmonics present in the X-ray beam. Samples were mixed with cellulose and pressed into wafers. Immediately preceding the recording of XAS spectra samples were cooled rapidly to liquid nitrogen temperature. The spectra $\mu(k)$ were measured in transmission mode using ionization chambers. A metal foil (between the second and the third ionization chamber) was measured at the same time for energy calibration purposes. Data treatment was carried out using the software package VIPER.[24] For background subtraction a Victoreen polynomial was fitted to the pre-edge region. A smooth atomic background $\mu_0(k)$ was evaluated using smoothed cubic splines. The radial distribution function FT[$k^2\chi(k)$] was obtained by Fourier transformation of the k^2-weighted experimental function $\chi(k) = (\mu(k) - \mu_0(k))/\mu_0(k)$ multiplied by a Bessel window. Duplicate spectra were recorded to ensure data reproducibility.

Determination of the Copper Surface Area. Reactive frontal chromatography using N_2O (1 vol. % diluted in He) as reactive gas was employed for determination of the accessible Cu surface area at 240 °C as described in detail in the literature.[20]

Methanol Catalysis Test. Typically a 100 mg amount of the samples was heated to 175 °C (linear ramp of 1 K/min) under H_2 (2%) diluted in He and kept at 175 °C for 15 h overnight. The samples were then heated to 240 °C (1K/min) and kept at 240 °C under H_2 (100%) for 30 min. Then the Cu surface was determined by N_2O-RFC (see above). Subsequently, the catalytic test was performed using a standard gas mixture for methanol synthesis of H_2 (72%), CO_2 (4%), CO (10%), and He (14%) with 50 mL/min at 220 °C, which is optimized for comparison of model catalysts with industrial reference samples. The produced methanol was continuously recorded by calibrated QMS. The method and experimental setup is described in detail in the literature.[25]

Results and Discussion

Loading MOF-5 With Cu Nanoparticles: Cu@MOF-5. The gas-phase loading of MOF-5 with [CpCu(PMe_3)] and [CpCu(CN^{t}Bu)] to yield the inclusion compounds $[CpCu(PMe_3)]_2$@MOF-5 (**1**) and [CpCu(CN^{t}Bu)]@MOF-5

(24) Klementiev, K. V. *J. Phys. D: Appl. Phys.* **2001**, *34*, 209.
(25) (a) Hinrichsen, O.; Genger, T.; Muhler, M. *Chem. Eng. Technol.* **2000**, *11*, 956. (b) Bielawa, H.; Kurtz, M.; Genger, T.; Hinrichsen, O. *Ind. Eng. Chem. Res.* **2001**, *40*, 2793. (c) Kurtz, M.; Bauer, N.; Buescher, C.; Wilmer, H.; Hinrichsen, O.; Becker, R.; Rabe, S.; Merz, K.; Driess, M.; Fischer, R. A.; Muhler, M. *Catal. Lett.* **2004**, *92*, 49.

(**2**) has been described in detail previously.[16] In the case of **1**, two precursor molecules are included per formula unit of MOF-5, while in the case of **2** only one molecule is included. The number of included precursor molecules depends on the size and shape of the precursor molecules, thermodynamics of the adsorption, interaction of the precursors with each other (i.e., their packing properties), and conditions of the loading experiment itself.[16] The distribution of the included precursor molecules over the cavities and adsorption sites may be random; however, some ordering or preferred clustering may be possible as discussed in the case of $[Cp_2Fe]_n$@MOF-5.[16,26] The intermediates **1** and **2** can be converted into the respective materials Cu@MOF-5 by photoassisted thermolysis at 90−100 °C under inert gas or purely thermal hydrogenolysis at 200−220 °C or photoassisted hydrogenolysis. Table 1 shows the Cu loading (wt %) of Cu@MOF-5 in comparison to the Cu content of **1** and **2**. A loading of about 10−11 wt % Cu in the final material Cu@MOF-5 was obtained with one loading cycle, which is a bit lower than expected from the copper content of the starting inclusion compound **1** or **2**. The reason may be that some precursor is desorbed during decomposition. N_2 absorption studies revealed type I isotherms and gave values of 1000−1100 $m^2 \cdot g^{-1}$ for the equivalent Langmuir surface, providing evidence for still highly porous materials Cu@MOF-5 derived from both **1** and **2**. For Cu@MOF-5 derived from **2**, hydrocarbon impurities (i.e., ligands or fragments from decomposition of the precursor) were almost not detectable by FTIR and ^{13}C-MAS NMR. In particular, the intense ν(CN) stretching vibration of the ^{t}BuNC ligand at 2172 cm^{-1} dominating the FTIR spectrum of **2** was nearly completely gone. However, the Cu@MOF-5 material derived from **1** showed some notoriously remaining PMe_3 in the ^{13}C- and ^{31}P-MAS NMR. FTIR indicates some additional ν(CH) absorptions in the aliphatic region at 2900−3200 cm^{-1} too. The nature of the retained P species is not clear; however, weakly physisorbed PMe_3 and $OPMe_3$, as likely impurities, can be ruled out based on the ^{31}P NMR shifts. It should be noted here that the MOF-5 structure collapses when treated with an excess of gaseous PMe_3.

Figure 1 compares the X-ray powder diffraction patterns of the parent MOF-5 (desolvated, activated) under Ar (capillary mode) with different samples Cu@MOF-5 prepared from **1** and **2** under various conditions including the TEM of a representative sample. It is clearly seen that the characteristic reflection pattern of the crystalline MOF-5 host material is nicely retained. However, the relative intensities and fwhms of some peaks have changed to some extent. These are known effects associated with the adsorption/desorption of molecules or the imbedding on nanoclusters inside porous crystalline materials such as zeolites, mesoporous silica, and coordination polymers such as MOFs.[27] The PXRD pattern of as-synthesized MOF-5 containing the solvent molecules diethylformamide shows slight differences as compared with the desolvated and activated MOF-5.[28] However, the faint changes in peak positions and some broadening of the line widths may also indicate a very small deformation or defects of the network. The structural quality of the matrix of Cu@MOF-5 derived from **2** appears to be better (sharper peaks) as compared with the material derived from **1**. This effect may be caused by the interaction of PMe_3 with the MOF-5 matrix (i.e., $Zn^{2+}-PMe_3$ coordination and displacement of bdc linkers), which may lead to some local defects. However, analysis of these details is beyond the scope of the work presented here. The PXRD also shows broad and weak reflections arising from nanoscale Cu particles. A rough size estimation based on a profile analysis (pseudo Voigt) and the Scherrer equation gives values of 3.5 (±0.5) nm. Particles with crystallite domains (coherence lengths) of that size are clearly larger as the typical dimension of the larger cavity of MOF-5 with a van der Waals diameter of 1.5 nm.[5] However, PXRD is comparably insensitive for such small nanocrystallites. Transmission electron micrographs of the obtained Cu@MOF-5 materials give evidence for Cu particles of 1−3 nm homogeneously distributed over the matrix (Figure 1). No particles or agglomerates outside the matrix were seen. However, TEM images are a 2D projection of the 3D distribution, and particle size determination without TEM tomography is again difficult. More or less spherical Cu nanoparticles with sizes around 1.5 nm matching the dimensions of the cavity are likely to consist of about 150 Cu atoms; particles of about 3 nm in size may be built from 1500 Cu atoms (e.g., an ideal three-shell icosahedral metal cluster consists of 147 atoms).[29] From the composition of the starting inclusion compounds **1** and **2** with two and one precursor molecule per formula unit and the measured Cu loading of 10−11 wt % it follows that certainly not more than 1% of the cavities are likely to be filled and/or directly affected by formation of the Cu nanoparticles inside the matrix. Thus, the effect of local structural damage caused by formation of the Cu nanoparticles is likely to be small. This reasoning agrees with the observed PXRD, which reveal a rather intact structure of the MOF-5.

A representative sample Cu@MOF-5 derived from **1** was further characterized by X-ray absorption spectroscopy (XAS). The XANES and EXAFS features at the Zn Kα edge (Figure 2) expectedly reveal Zn^{2+} coordinated by O^{2-} in a tetrahedral fashion in the first shell similar to ZnO. However, closer inspection shows differences. The higher shells are clearly missing. The measured EXAFS were compared with calculated spectra using a model of the secondary building unit of the type $[Zn_4O(OOC)_6]$ for coordination of the Zn^{2+} ions (see Supporting Information). The matching of the calculated and measured spectra substantiates the conclusions drawn from the PXRD that the structural identity of the MOF-5 matrix is largely unaffected.

Similar XAS measurements at the Cu Kα edge were performed aiming at a characterization of the embedded Cu

(26) Kim, H.; Chun, H.; Kim, G.; Lee, H.; Kim, K. *Chem. Commun.* **2006**, *26*, 2759.
(27) Marler, B.; Oberhagemann, U.; Vortmann, S.; Gies, H. *Microporous Mater.* **1996**, *6*, 375.
(28) Hafizovic, J.; Bjørgen, M.; Olsbye, U.; Dietzel, P. D. C.; Bordiga, S.; Prestipino, C.; Lamberti, C.; Lillerud, K. P. *J. Am. Chem. Soc.* **2007**, *129*, 3612.
(29) Aiken, J. D.; Finke, R. G. *J. Mol. Catal. A: Chem.* **1999**, *145*, 1.

Table 2. Relevant Catalytic Properties of Catalysts for Methanol Synthesis

	production rate		metal surface	wt % metal	
catalyst	$\mu mol_{MeOH} \cdot g^{-1}{}_{cat} \cdot h^{-1}$	$\mu mol_{MeOH} \cdot g^{-1}{}_{Cu} \cdot h^{-1}$	$m^2{}_{Cu} \cdot g^{-1}{}_{cat}$	Cu	Zn
Cu@MOF-5	70	508	6.3	13.8	29.0
(Cu/ZnO)@MOF-5 (method A)	212 (initial), 12 (end)	20 100 (initial), 3670 (end)	<0.5	1.4	40.1
(Cu/ZnO)@MOF-5 (method B)	40	640	0.9	7.6	43.0
(Cu/ZnO)@MCM-41[18]	36	387	6.2	9.3	10.4
(Cu/ZnO)@MCM-48[18]	130	1226	5.8	10.6	21.9
$Cu/ZnO/Al_2O_3$[18]	404	673	20−25	60	30

particles. The measured XANES and EXAFS are compared with reference samples of bulk Cu, CuO, and Cu_2O (Figure 3). The XANES of the Cu@MOF-5 rules out the presence of Cu^{2+}. Traces of Cu^+, e.g., Cu_2O species, can bee seen in the EXAFS. A shoulder at 1.5 Å (uncorrected) is assigned a Cu^+-O shell. However, both XANES and EXAFS clearly reveal that the sample contains mainly Cu(0). The low amplitude of the Fourier transform FT(χ) (see Supporting Information) indicates small particles with some ordering up to 8 Å. An average coordination number of 7.1 (±0.3) was extracted from the modeling. A diameter of 9 (±0.4) Å was estimated based on the Borowski method for spherical monodispersed particles.[30] This estimation is well below the crystallite size estimation obtained from PXRD but matches the size of the cavities much better. In contrast to PXRD, XAS is more sensitive for small particles (i.e., nearest neighbor interactions). It is thus likely that the Cu@MOF-5 sample is polydisperse to some extent with a *minority* of larger Cu particles (3 nm) giving rise to the broad peaks in the PXRD and a *majority* of smaller particles (1 nm) dominating the EXAFS. These conclusions are in agreement with the TEM images and previous reports on Cu@MCM-41/48 systems.[18] Finally, the Cu surface area of a representative sample Cu@MOF-5 was determined by N_2O reactive frontal chromatography[31] (eq 1), and values around 6.3 (±0.5) m^2/g_{sample}, which corresponds to about 65 m^2/g_{Cu}, were measured reproducibly. Typical reference samples of binary Cu/ZnO catalysts and commercial ternary $Cu/ZnO/Al_2O_3$ catalysts show values of 20−25 $m^2/g_{Catalyst}$ and 40−50 m^2/g_{Cu}, respectively (Table 2).[18]

$$N_2O(g) + 2Cu(s) \rightarrow N_2(g) + (Cu - O - Cu)(s) \qquad (1)$$

Redox Chemistry of Cu@MOF-5. Determination of the Cu surface area above is based on the controlled, stoichiometric reaction of N_2O with surface Cu atoms according to eq 1. One mole of N_2 (detected by GC) is equivalent to 2 mol of surface Cu atoms.[31] Figure 4 shows the PXRD patterns together with images of the sample at different stages of reaction. A color change is seen when a Cu@MOF-5 sample is surface oxidized with N_2O (0.5%, diluted in Ar, ambient pressure) and finally reduced with hydrogen (100%) on a preparative scale. Even at room temperature (25 °C) the initially red-brown Cu@MOF-5 turns black when treated with the N_2O. Oxidation at elevated temperatures of 170 °C leads to a green-black appearance and at 220 °C, which is the typical setting for the N_2O RFC, a deep green color results. Subsequent reduction with H_2 (100%) at 220 °C gives back the initial red-brown-colored material. The associated PXRD patterns (Figure 4) show the reversibility of the oxidation/reduction cycle with the crystallite size seemingly unaffected. Formation of Cu_2O is indicated by some broad structures rising from the background noise at the expected 2θ values for Cu_2O with the MOF reflections as superposition (Figure 4b). We suggest that these structures may arise from oxidation of very small Cu particles (≤1.5 nm) exhibiting a very high surface/volume ratio and thus may tend to be completely oxidized. The larger particles may be surface oxidized only. The corresponding XAS studies at the Cu Kα edge (Figure 3) substantiate the hypothesis of a partial (surface) oxidation of the Cu nanoparticles inside the MOF-5. The XANES and EXAFS match with a major Cu(0) contribution, showing a superposition of a minor contribution of a Cu^+-O contact similar to a Cu_2O reference. CuO can be ruled out. N_2 adsorption measurements after the oxidation/reduction cycles gave values of 1000 $m^2 \cdot g^{-1}$, again indicating that the Cu@MOF-5 material is retained without significant changes. However, the attempted total oxidation of the Cu to Cu_2O or CuO particles inside MOF-5 using dry O_2 (0.5%, in Ar) at 25 °C for 2 h or exposure of Cu@MOF-5 to the ambient atmosphere (moist air) led to complete collapse of the MOF-5 matrix with a very low remaining porosity of 10−20 $m^2 \cdot g^{-1}$. A similar behavior was observed when **1** was treated directly with dry O_2 at 190 °C.

Catalytic Properties of Cu@MOF-5 for Methanol Synthesis. The above-described samples Cu@MOF-5 have been tested as catalysts for methanol synthesis using a setup described in detail elsewhere.[12] A stable productivity of 70 $\mu mol_{MeOH} \cdot g^{-1}{}_{cat} \cdot h^{-1}$ was reproducibly measured at 1 atm pressure for a freshly prepared Cu@MOF-5 sample with a Cu loading of 13.8 wt % using a standard synthesis gas

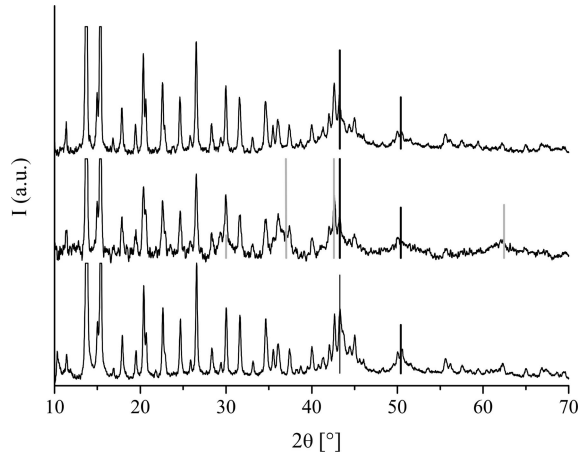

Figure 4. Powder X-ray diffraction patterns of (a) Cu@MOF-5 (as prepared), (b) (Cu/Cu_2O)@MOF-5, and (c) Cu@MOF-5 (after reduction of b) with H_2, 220 °C (marked reflections: black, Cu JPDS No. 4-0836; gray, Cu_2O JPDS No. 00-035-1091).

(30) Borowski, M. *J. Phys. IV Fr. 7* **1997**, C2−259.
(31) Hinrichsen, O.; Genger, T.; Muhler, M. *Chem. Ing. Tech.* **2000**, *72*, 94.

mixture (Experimental Section). This observation is surprising since pure copper without the promoting effect of ZnO usually shows little or no activity at all.[32] The measured productivity compares with typical Cu/ZnO/matrix catalysts (Table 2) and reaches about 17% of the activity of a ternary industrial reference catalyst ($Cu/ZnO/Al_2O_3$).[13] Surfactant-stabilized pure copper colloids are inactive in methanol synthesis despite the accessibility of the Cu surface for CO/H_2. However, ZnO-promoted Cu nanoparticles dispersed as colloids are quite active, reaching the level of industrial reference samples in a slurry reactor.[33] However, for Cu@MOF-5 no indication for formation of ZnO species during the catalytic tests were found: ^{13}C-MAS NMR, PXRD, and N_2 adsorption studies before and after the catalytic test matched (see Supporting Information). Since the PXRD gave no hint at all for formation of nanocrystalline ZnO species, an XAS study will also not be able to unambiguously discriminate between the $[Zn_4O(OOC)_6]$ species of the largely intact MOF and the possibly formed other ZnO species of certainly low concentration and very low aggregation size. The same is true for UV−vis studies before and after the catalytic cycles. Nevertheless, the accessible data cannot rule out that some promoting ZnO species may be formed during the catalytic reaction. We were thus led to study the possibility to load the MOF-5 host matrix with both Cu and ZnO nanoparticles and test the catalytic activity of a material denoted as (Cu/ZnO)@MOF-5. In order to achieve this, however, the loading of MOF-5 with ZnO was investigated first.

Loading MOF-5 with ZnO Nanoparticles, ZnO@MOF-5. Diethylzinc is a pyrophoric, highly reactive compound in contact with moist air and represents a well established precursor for ZnO materials as thin films, nanoparticles, and nanopowders and as well ZnO/matrix nanocomposites.[19,33,34] Alternative ZnO precursors such as $[Zn(acac)_2]$[35] or $[(RZnOR')_4]$[36] have been considered but not selected because of the rather harsh conditions (>200 °C) needed for their decomposition into ZnO. Thus, a straightforward concept for preparation of the target ZnO@MOF-5 material is the controlled hydrolysis/oxidation of the inclusion compounds $[ZnEt_2]_n$@MOF-5. These materials can be derived by adsorption of $ZnEt_2$ vapor from the gas phase under strict exclusion of oxygen and moisture (see Experimental Section). Reversible adsorption/desorption of $ZnEt_2$ is possible, leaving the MOF-5 host material unchanged.[16] This observation is surprising since $ZnEt_2$ could in principle react with the $Zn_4O(bdc)_6$ connector units and break down the network, which in fact happens if a MOF-5 sample is treated with excess neat, liquid $ZnEt_2$ at room temperature. As noted in detail in the Experimental Section, the samples $[ZnEt_2]_n$@MOF-5 were converted into ZnO@MOF-5 following two different methods A and B. Method A involves a gentle exposure of $[ZnEt_2]_n$@MOF-5 to moist air at room temperature or with cooling and thus involves a combination of hydrolysis with oxidation. Method A was developed aiming at the ^{17}O-labeling studies using $H_2{}^{17}O$ as discussed in the next section. Method B rather avoids moisture as rigorously as possible and uses dry oxygen (4 vol. % in Ar) as reactant at room temperature. The compositions of the finally obtained materials ZnO@MOF-5 by either method were determined by combustion analysis (C, H) and atomic absorption spectroscopy (Zn) after an annealing step at 250 °C (dynamic vacuum at 10^{-3} mbar, 6 h). Thus, the measured loadings with ZnO reflect the initial loadings with $ZnEt_2$ (which were not determined independently). For example, from the elemental analysis of the samples ZnO@MOF-5 prepared by method A (Table 1) a loading of about 17.5 wt % ZnO was deduced which nicely corresponds to $[ZnEt_2]_2$@MOF-5 ($n = 2$) as the composition of the starting material. The obtained ZnO loadings range from about one formula unit ZnO (9.6 wt %) to a maximum of five formula units of ZnO (35 wt %) with the parameter n of $[ZnEt_2]_n$@MOF-5 ranging between 1 and 5, respectively. FTIR and ^{1}H/^{13}C-MAS NMR gave evidence of the quantitative release of aliphatic hydrocarbon species. Only traces of Zn−Et species or other species with ethyl groups were detected. Surface areas of 860−900 $m^2 \cdot g^{-1}$ (Langmuir model) were determined for the annealed samples prepared by the wet method A irrespective of the loading with 17.5 or 35 wt % ZnO. However, the as-synthesized (not annealed) samples, denoted as as-ZnO@MOF-5, revealed a much less specific surface area of about 600 $m^2 \cdot g^{-1}$. This difference is attributed to incomplete desorption of organic byproduct and in particular water before the N_2 adsorption studies. The samples ZnO@MOF-5 prepared by the dry method B showed systematically larger surface areas (e.g., 1750 $m^2 \cdot g^{-1}$ for 35 wt % ZnO).

The obtained ZnO@MOF-5 materials were further characterized by PXRD and TEM. Figure 5 (left) displays the PXRD comparison between the empty MOF-5 reference material (Figure 5a), a typical $ZnEt_2$-loaded intermediate (Figure 5b), and the various ZnO-loaded MOF-5 product samples (Figure 5c−f) with a nanocrystalline ZnO reference sample (Figure 5g). The smooth hydrolysis of $ZnEt_2$ inside the cavities of MOF-5 according to method A leads to a sample as-ZnO@MOF-5 (Figure 5c) which does not show any ZnO-related X-ray diffraction peaks but still reveals all reflexes characteristic for the MOF-5 crystal structure without changing the relative intensities but with a somewhat lower signal-to-noise ratio. Upon annealing at 250 °C for 6 h a broad structure develops at $2\theta = 30-37°$ with the indication of the characteristic signature for hexagonal ZnO (Figure 5d) as deduced from the comparison with the PRXD pattern of ZnO reference sample (Figure 5g) of Figure 5. The as-ZnO@MOF-5 (Figure 5e) derived by dry oxidation before

(32) (a) Kurtz, M.; Wilmer, H.; Genger, T.; Hinrichsen, O.; Muhler, M. *Catal. Lett.* **2003**, *86*, 77. (b) Kurtz, M.; Bauer, N.; Buscher, C.; Wilmer, H.; Hinrichsen, O.; Becker, R.; Rabe, S.; Merz, K.; Driess, M.; Fischer, R. A.; Muhler, M. *Catal. Lett.* **2004**, *92*, 49.

(33) (a) Schroeter, M. K.; Khodeir, L.; van den Berg, M. W. E.; Hikov, T.; Cokoja, M.; Miao, S.; Gruenert, W.; Muhler, M.; Fischer, R. A. *Chem. Commun.* **2006**, *23*, 2498. (b) Schröter, M. K.; Khodeir, L.; Löffler, E.; Muhler, M.; Fischer, R. A. *Langmuir* **2004**, *20*, 9453. (c) Hambrock, J.; Becker, R.; Birkner, A.; Weiss, J.; Fischer, R. A. *Chem. Commun.* **2002**, 68.

(34) Wolden, C. A. *Plasma Chem. Plasma Process.* **2005**, *25*, 169.

(35) Polarz, S.; Neues, F.; van den Berg, M. W. E.; Gruenert, W.; Khodeir, L.; Muhler, M. J. *Am. Chem. Soc.* **2005**, *125*, 2018.

(36) (a) Driess, M.; Merz, K.; Schoenen, R. *Organometallics* **2007**, *26*, 2133. (b) Perez, L. M.; Aguilar-Frutis, M.; Zelaya-Angel, O.; Aguirre, N. M. *Phys. Status Solidi A* **2006**, *203*, 2411. (c) Shibata, S.; Ohta, M. *J. Mol. Struct.* **1981**, *77*, 265.

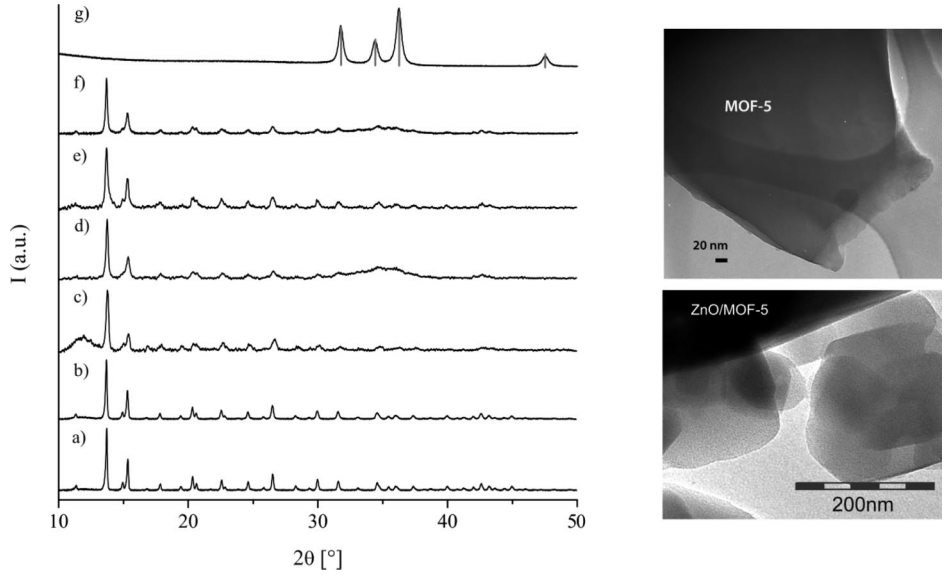

Figure 5. (Left) Powder X-ray diffraction patterns of MOF-5 (a), [$ZnEt_2$]@MOF-5 (b), as-ZnO@MOF-5 (as synthesized by the wet method) (c), ZnO@MOF-5 (after annealing and derived by the wet method) (d), as-ZnO@MOF-5 (as synthesized by the dry method) (e), ZnO@MOF-5 (after annealing and derived by the dry method) (f), and ZnO reference sample obtained from controlled hydrolysis of $ZnEt_2$ and annealing in air (g). The positions of the characteristic reflections of hexagonal ZnO are marked. (Right) TEM images of unloaded MOF-5 (a) and ZnO@MOF-5 (f, after annealing and derived by the dry method).

annealing and the annealed sample (Figure 5f) show similar features as the corresponding samples (Figure 5c) before and (Figure 5d) after annealing derived by the wet method. A size estimation using profile fitting and the Scherrer equation based on representative samples ZnO@MOF-5 (d and f, Figure 5) gives about 4 (±0.5) nm as an upper limit of the ZnO crystallite domains. The crystallize size of the reference sample (Figure 5g) was estimated to 22 (±1) nm by the same method. Clearly the PXRD pattern of the annealed samples ZnO@MOF-5 (d and f, Figure 5) reveal significant deviations from the parent pattern of empty MOF-5. However, again all characteristic diffraction peaks are visible but broadened and the signal-to-noise ratio is further reduced as compared with c and e of Figure 5. Transmission electron microscopic studies (TEM) were undertaken (Figure 5, right). The comparison with empty MOF-5 indicated the loading effect by some enhanced contrast. A size estimation of the barely visible structures was not possible.

The UV absorption edge at 370−380 nm of Figure 6d is characteristic for polycrystalline ZnO materials with crystallize sizes well above the quantum size limit of 4 nm.[37] Empty MOF-5 (Figure 6a) is transparent in the region typical for ZnO absorptions and shows a steep absorption at 280 nm due to the $\pi \rightarrow \pi^*$ excitation of the terephthalic acid linkers. The weak structure at 365 nm has been assigned to the inorganic Zn_4O moiety (SBU) of the MOF-5 framework.[38] The two other traces (Figure 6b and 6c) clearly show a blue shift of the onset of the ZnO-related absorptions. From the comparison with literature information on UV absorption data of ZnO nanoparticles[37] it may be concluded that the as-ZnO@MOF-5 sample contains ZnO species of a size around 2−2.5 nm while the UV absorption of the annealed

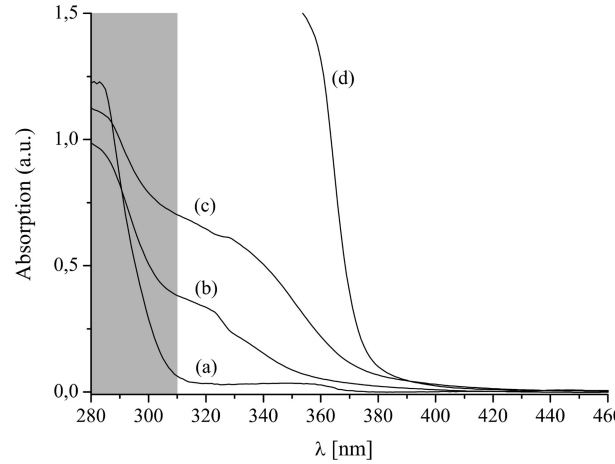

Figure 6. Corresponding UV absorption spectra of the samples as-ZnO@MOF-5 (b) and the annealed ZnO@MOF-5 (c) derived by method A in comparison with the MOF-5 starting materials (a) and the nanocrystalline ZnO reference material (d). The UV absorption spectrum of ZnO@MOF-5 derived by method B shows no significant difference from c and is left for purposes of clarity. The adsorption region of the organic part of MOF-5 ($\pi \rightarrow \pi^*$) is marked gray (a).

ZnO@MOF-5 points to particles around 4 nm in congruence with the respective PXRD data. Thus, the ZnO particles are likely to extend over several cavities of the MOF-5 as shown in the suggested model of Figure 7, which certainly causes structural defects of the matrix (i.e., line broadening in the PXRD).

^{17}O-Labeling Studies of ZnO@MOF-5. Conversion of $ZnEt_2$ into ZnO inside the cavities by hydrolysis/oxidation as described above may in principle be accompanied by chemical interactions of intermediate zinc oxide/hydroxide species with the MOF-5 matrix. In addition, the formed ZnO nanoclusters and/or the intermediate zinc oxide/hydroxide clusters may interact with the bdc linkers leading to disintegration of the network. Note, that MOF-5 and other carboxylic acid-based MOF phases can be synthesized from

(37) Haase, M.; Weller, H.; Henglein, A. *J. Phys. Chem.* **1988**, *92*, 42.
(38) Bordiga, S.; Lamberti, C.; Ricchiardi, G.; Regli, L.; Bonino, F.; Damin, A.; Lillerud, K.-P.; Bjorgen, M.; Zecchina, A. *Chem. Commun.* **2004**, 2300.

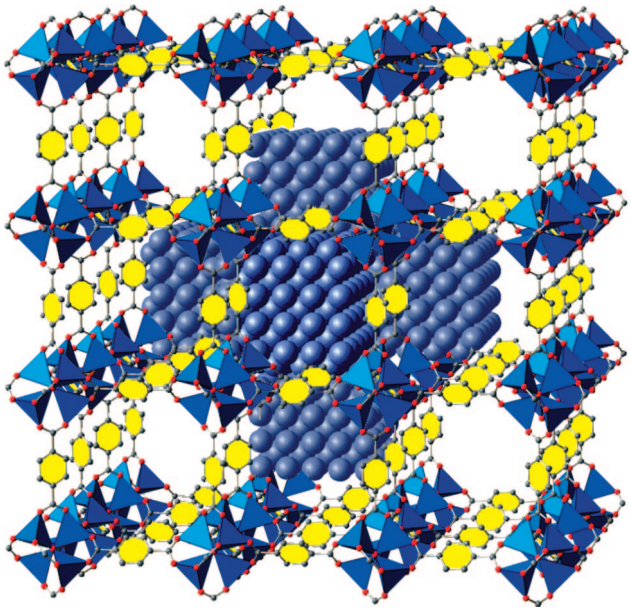

Figure 7. Possible imbedding of ZnO nanoparticles of 3−4 nm inside MOF-5 extending over several cavities with typical diameters of 1.5 nm. The growth of that large ZnO species certainly causes local damage to the MOF matrix, which is indicated by line broadening in the PXRD (Figure 5).

ZnO and the organic acid under certain conditions.[39,40] In addition, MOF-5 is known to be water sensitive and the lattice will collapse when water is adsorbed beyond a level of 5 wt %.[41] We were thus lead to use ^{17}O labeling to distinguish between the Zn−O moieties of the framework and the embedded (nanoscale) ZnO-type species.

Several samples of selectively ^{17}O-labeled MOF-5 were synthesized. Preparation of ^{17}O-labeled terephthalic acid reaching a level of about 8% ^{17}O enrichment was done following literature methods by treating a suspension of terephthalic acid in DMSO with HCl-saturated $H_2{}^{17}O$ (30% ^{17}O) for 24 h at reflux.[42] The tetrahedral building unit Zn_4O contains an oxide ion which is incorporated from deprotonated water molecules during the MOF synthesis introduced by the typical zinc source $Zn(NO_3)_2 \cdot 4H_2O$.[43] Addition of stoichiometric amounts of $H_2{}^{17}O$ (30%) to the DEF solution at the beginning of the MOF synthesis allows enrichment of the Zn_4O unit. Accordingly, we derived three labeled samples: (i) both sites, i.e., ^{17}O-MOF-5^{ab}, (ii) the carboxylic site only, i.e., ^{17}O-MOF-5^{a}, and (iii) the Zn_4O site only, i.e., ^{17}O-MOF-5^{b}. Solid-state MAS NMR of ^{17}O-MOF-5^{ab} (see Supporting Information) reveals the ^{17}O resonances of both sites at $\delta = 202$ ppm for the carboxylic groups (a site) and $\delta = -50$ ppm for the Zn_4O unit (b site). These ^{17}O data are quite typical for basic zinc carboxylates and match literature data.[44] Interestingly, there is *no exchange* between the labeling of the a and the b site during formation of the MOF network and crystallization from the mother liquor. The NMR spectra of a MOF sample, which was synthesized with ^{17}O-labeled terephthalic acid in the *absence* of additional $H_2{}^{17}O$ shows the a site at 202 ppm only. Correspondingly, only the b site at −50 ppm shows up if normal terephthalic acid is used in combination with addition of $H_2{}^{17}O$ during MOF synthesis. Incorporation of ^{17}O from $H_2{}^{17}O$ into terephthalic acid is very slow under basic conditions.[42] The other analytical and spectroscopic parameters of the labeled MOF-5 samples fully matched the reported data of typical MOF-5 (see Experimental Section). Following method A for the loading of MOF-5 with ZnO species and using either selectively ^{17}O-labeled MOF-5 samples as host matrix and regular water for the hydrolysis of adsorbed $ZnEt_2$ or regular MOF-5 as host matrix and ^{17}O-enriched water for the hydrolysis of the included $ZnEt_2$ the following ^{17}O-labeled samples were prepared: (i) $Zn^{17}O$@MOF-5, (ii) ZnO@^{17}O-MOF-5^{ab}, and (iii) $Zn^{17}O$@^{17}O-MOF-5^{ab}. The corresponding solid-state MAS ^{17}O NMR spectra in the range from 0 to −80 ppm are depicted in Figure 8 together with the spectrum of the nanocrystalline $Zn^{17}O$ reference sample. In addition, neither the signal at 202 ppm (a site, carboxylate) nor the signal at −50 ppm (b site, Zn_4O) showed up in the case of $Zn^{17}O$@MOF-5. This gives further evidence that hydrolysis of $ZnEt_2$ and subsequent condensation of $Zn(OH)_2$ species to form ZnO takes place without significant exchange of ^{17}O labels between the framework and the growing ZnO species. Annealing at 250 °C for 6 h did not change the spectra. The same result was obtained using single-site-labeled ^{17}O-MOF-5^{a} and ^{17}O-MOF-5^{b} samples.

Loading with Cu and ZnO: Catalytic Properties of (Cu/ZnO)@MOF-5. Treatment of **1** with gaseous $ZnEt_2$ at 25 °C gave a material {[CpCu(PMe_3)]/$ZnEt_2$}@MOF-5 in which ^{13}C-MAS NMR spectrum nicely showed both organometallic precursors being adsorbed unchanged (see Supporting Information) and the PXRD revealed the unaffected MOF-5 matrix. However, all attempts to pyrolyse, photolyze, hydrolyze, or oxidize this material under various conditions lead to undesired quantitative collapse of the framework with no remaining ordering (no XRD reflections) and very low specific surface areas of 20 $m^2 \cdot g^{-1}$. Cu@MOF-5 can be loaded with $ZnEt_2$ without disintegration of the MOF-5 matrix. However, as soon as hydrolysis/oxidation of the obtained $ZnEt_2$/Cu@MOF-5 material is attempted, following the protocols for the preparation of ZnO@MOF-5, the matrix collapsed surprisingly. Finally, a sample of as-ZnO@MOF-5 (600 $m^2 \cdot g^{-1}$) derived by method A was loaded with [CpCu(PMe_3)] using the standard method of gas-phase infiltration similar to the preparation of **1** and **2**. ^{13}C-MAS NMR and PXRD gave evidence of unchanged adsorption of the Cu precursor and an intact MOF-5 matrix. Subsequent conversion under hydrogen (100%) at 220 °C (5 h) afforded a weakly brownish material of 820 $m^2 \cdot g^{-1}$ surface area with 1.4 wt % Cu and 9.9 wt % ZnO, which still showed the typical signature of MOF-5 in the PXRD (Figure 9a). However, the obtained Cu loading was quite low as compared with the Cu@MOF-5 samples (10−11 wt % Cu). The specific Cu surface was not detectable by N_2O RFC,

(39) Clegg, W.; Harbron, D. R.; Homan, C. D.; Hunt, P. A.; Little, I. R.; Straughan, B. P. *Inorg. Chim. Acta* **1991**, *186*, 51.
(40) Berkesi, O.; Dreveni, I.; Andor, J. A.; Goggin, P. L. *Inorg. Chim. Acta* **1991**, *181*, 285.
(41) Greathouse, J. A.; Allendorf, M. D. *J. Am. Chem. Soc.* **2006**, *106*, 10678.
(42) Gerothanassis, I. P.; Hunston, R.; Lauterwein, J. *Helv. Chim. Acta* **1982**, *65*, 1764.
(43) Hausdorf, S.; Baitalow, F.; Seidel, J.; Mertens, F. O. R. L. *J. Phys. Chem. A* **2007**, *111*, 4259.
(44) Schramm, S.; Oldfield, E. *J. Am. Chem. Soc.* **1984**, *106*, 2502.

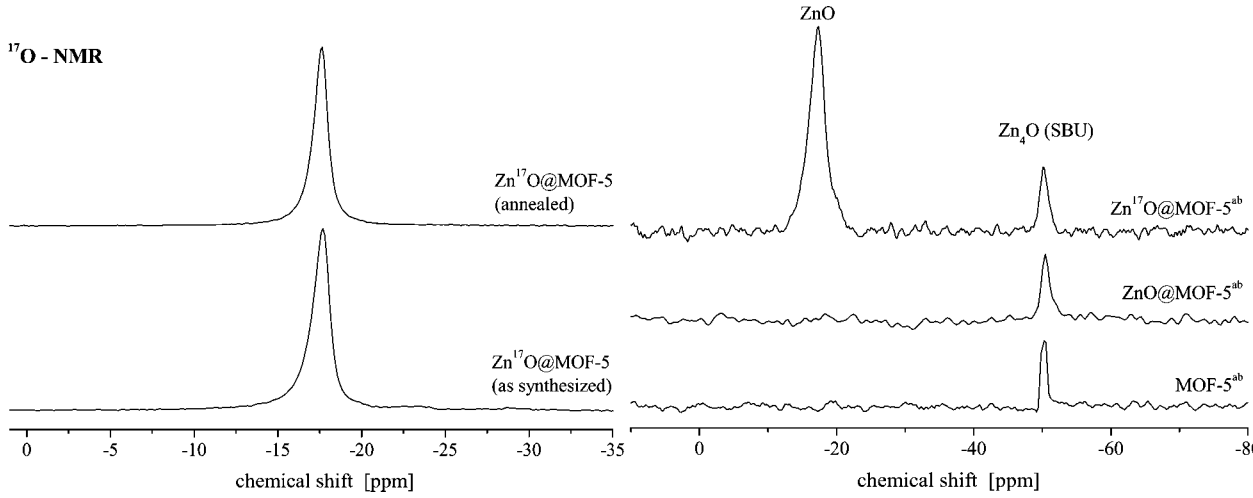

Figure 8. (Left) Annealing of as-[Zn^{17}O]$_2$@MOF-5 did not affect the ^{17}O shift of incorporated zinc oxide. (Right) Characteristic region of the ^{17}O NMR spectrum for ZnO and Zn$_4$O (SBU) species of labeled ZnO@MOF-5^{ab} and Zn^{17}O@MOF^{ab} samples. The missing signal for ZnO in the sample ZnO@MOF-5^{ab} indicates that there is no significant exchange of labeling.

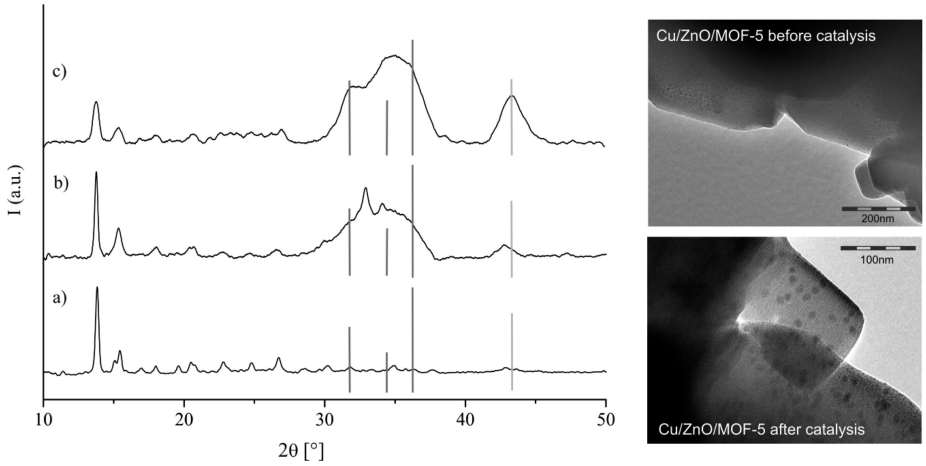

Figure 9. (Left) Powder X-ray diffraction patterns of as-Cu/ZnO@MOF-5 before catalytic testing (a), Cu/ZnO@MOF-5 (derived by the wet method and use of [CpCu(PMe$_3$)]) after catalytic testing (b), and Cu/ZnO@MOF-5 (derived by the dry method and use of [CpCu(CN^{t}Bu)]) after catalytic testing. Weak reflexes for MOF-5 (c) present the collapsed MOF-5 matrix after catalytic testing. (Lines: dark gray, ZnO JPDS No. 00-036-1451; light gray, Cu JPDS No. 00-004-0836). (Right) TEM images of the Cu/ZnO@MOF-5 material derived by the dry method and use of [CpCu(CN^{t}Bu)] before catalysis (above) and after catalytic testing (below).

which correlates to values below the detection limit of 0.5 $m^2 \cdot g^{-1}$. Nevertheless, the catalyst activity in methanol synthesis was determined similar to Cu@MOF-5 before. Remarkably high *initial* activities of 212 $\mu mol_{MeOH} \cdot g^{-1}{}_{cat} \cdot h^{-1}$ were measured after 1 h on stream at 220 °C, but deactivation occurred gradually over a period of 20 h, stabilizing at a level of 12 $\mu mol_{MeOH} \cdot g^{-1}{}_{cat} \cdot h^{-1}$. The PXRD after the catalysis test gave evidence of a sintering of the ZnO material (Figure 9b) and further disintegration of the MOF-5 matrix. However, the N_2 absorption still revealed a remaining microporosity of 805 $m^2 \cdot g^{-1}$. The TEM image of the Cu/ZnO@MOF-5 material after the catalytic test revealed a clear sintering of the Cu particles. Using [CpCu(CN^{t}Bu)] instead of [CpCu(PMe$_3$)] for loading of a sample ZnO@MOF-5 (35 wt % ZnO; derived by method B) with an extended infiltration time of 48 h at 50 °C and subsequent annealing under hydrogen (100%) at 220 °C resulted in a material with an increased loading of 7.6 wt % Cu. However, the MOF-5 matrix collapsed during the catalytic test (final porosity of 340 $m^2 \cdot g^{-1}$) instantaneously. Again, TEM gave evidence for sintering of the Cu particles (Figure 9, right). The particle size determination by TEM before catalytic testing gave a size distribution between 1 and 3 nm, which is in the same range as derived for Cu@MOF-5 (Figure 1). After catalysis, Cu particles with a size up to 15−20 nm were observed. Expectedly, the measured productivity of 40 $\mu mol_{MeOH} \cdot g^{-1}{}_{cat} \cdot h^{-1}$ was low. Table 2 compares the productivities of several (Cu/ZnO)@matrix catalysts with the industrial reference system. However, care should be taken in comparing the given productivities. A key feature of active catalysts is a high specific Cu surface, i.e., a good Cu loading value (wt %) together with a high dispesion (small Cu particles) and high porosity (BET) of the matrix. Then, an additional promoting effect of ZnO species in direct interfacial contact with the Cu particles will lead to a good catalyst if no sintering takes place. The comparisons of Table 2 indicate some promoting effect of the ZnO component of the Cu/ZnO@MOF-5 samples unless the lower specific activity at the collapsed state of the matrix. A possible explanation for the observed ZnO sintering and collapse of

the MOF matrix may be the inevitable water−gas shift reaction which is catalyzed to some extent by the Cu/ZnO system under the reaction conditions due to the CO_2 content of the synthesis gas (4 vol. %). MOF-5 is known to be sensitive to traces of water above 4−5 wt % (which corresponds to 1−2 molecules of adsorbed water per cavity).[41] This CO_2 content in the synthesis gas is however necessary for the comparisons with the industrial reference system of Table 2. In addition, it is known from ZnO nanoparticle research that water and certain surfactants such as alcohols and carbonic acids effect or even catalyze the Ostwald ripening of ZnO.[45,46]

Summary and Conclusion

We demonstrated the loading of MOF-5 with nanocrystalline Cu of 1−3 nm in size with the majority of the particles likely to match the size of the larger cavities of 1.5 nm as deduced from the comparison of PXRD, TEM, and EXAFS data. Only a small fraction (∼1%) of the cavities is loaded, and the structural features of the MOF-5 matrix were almost unaffected, i.e., the remaining specific surface areas were still high (>1000 $m^2 \cdot g^{-1}$). The loading with nanocrystalline ZnO via hydrolysis/oxidation of included $ZnEt_2$ was demonstrated as well. However, even though ^{17}O-labeling studies did not give evidence for a likely interaction between the bdc linkers and the Zn−O species of the matrix with the Zn−O species of the imbedded ZnO particles, the obtained ZnO@MOF-5 materials revealed less structural integrity as judged from the PXRD patterns compared to Cu@MOF-5. However, some of the prepared ZnO@MOF-5 materials (method B) still showed high remaining porosity (up to 1750 $m^2 \cdot g^{-1}$) together with remarkably high ZnO loading of about 35 wt %. UV−vis spectroscopy gave evidence for ZnO in the size quantization regime. The reversible surface oxidation/reduction with N_2O/H_2 of Cu@MOF-5 was demonstrated, whose chemistry is the basis of determination of the accessible Cu surface area. A value of 6 $m^2 \cdot g^{-1}_{sample}$ was determined for a representative sample Cu@MOF-5 (13.8 wt % Cu; 65 $m^2 \cdot g^{-1}_{Cu}$). However, full oxidation of the Cu@MOF-5 aiming at a CuO@MOF-5 material lead to complete destruction of the MOF-5 matrix. Preparation of (Cu/ZnO)@MOF-5 was surprisingly difficult. Among various alternatives being tested, only the gas-phase infiltration of previously prepared ZnO@MOF-5 with [CpCuL] and subsequent annealing under hydrogen yielded samples with remaining MOF-5 structure (PXRD) and reasonable porosity (∼800 $m^2 \cdot g^{-1}$). The testing of the catalytic properties showed stable values of 70 $\mu mol_{MeOH} \cdot g^{-1}_{cat} \cdot h^{-1}$ for Cu@MOF-5 and an initially high activity of 212 $\mu mol_{MeOH} \cdot g^{-1}_{cat} \cdot h^{-1}$ for the promoted (Cu/ZnO)@MOF-5 material; the latter is about 60% of the productivity of an industrial reference catalyst. However, in contrast to Cu@MOF-5, the ZnO-promoted system was instable on stream due to sintering of the ZnO component, resulting in a final level of 40 $\mu mol_{MeOH} \cdot g^{-1}_{cat} \cdot h^{-1}$ (10% of the industrial reference). Taking into account the rather low Cu loading (1−8 wt %) and corresponding low Cu surface area (<1 $m^2 \cdot g^{-1}$) of both samples (Cu/ZnO)@MOF-5 as compared with the industrial catalyst (60 wt % Cu; 20−25 $m^2_{Cu} \cdot g^{-1}$), the measured productivities are still quite remarkable. The same was observed for Cu/ZnO@MCM-41/48 catalysts and correlated to a possibly very efficient interfacial contact between the Cu and ZnO nanophases.[17,18] The certainly interesting microscopic details of the particular Cu/ZnO interface could however not be addressed in this work here. However, the significantly enhanced (initial) catalytic activity of the sample (Cu/ZnO)@MOF-5 in comparison to Cu/MOF-5 indirectly substantiates the view that the catalytic activity of Cu@MOF-5 comes close to the intrinsic activity of nonpromoted, "naked" Cu nanoparticles, which are otherwise very difficult to chemically synthesize and stabilize in a size regime below 3 nm. Taken together our results demonstrate the potential of MOFs as matrices for stabilizing catalytically active nanoparticles (Cu) and even composites of nanoparticles (Cu/ZnO). We propose to view Cu@MOF-5 and (Cu/ZnO)@MOF-5 as a bridge between colloidal nanocatalysts on the one hand and the solid-state-supported catalysts employing zeolites, mesoporous silica, and related micro- and mesoporous matrices as support materials on the other side. However, the known instability of the MOF-5 itself, in particular, to traces of water, but possibly also toward metal oxide nanoparticles as suggested by our results, clearly limits its usefulness as support material in heterogeneous catalysis. Nevertheless, our results may be well transferable to other MOFs being more robust. For example, the imbedding of Cu nanoparticles into $[Cu_3btc_2]$ (HKUST-1)[47] should be possible, and similar studies of the kind described above may be interesting also with MOFs of the MIL series.[8]

Acknowledgment. This work was supported by the German Research Foundation (DFG) within the Research Centre "Metal Substrate Interaction in Heterogeneous Catalysis" (SFB-558). M.M. is grateful for the support by the Ruhr-University Research School. The authors wish to thank Dr. L. Khodeir for very valuable help with the catalytic measurements.

Supporting Information Available: Additional information. This material is available free of charge via the Internet at http://pubs.acs.org.

CM703339H

(45) Niederberger, M.; Garnweitner, G. *Chem. Eur. J.* **2006**, *12*, 7282.
(46) Kahn, M.; Monge, M.; Colliere, V.; Senocq, F.; Maisonnat, A.; Chaudret, B. *Adv. Func. Mater.* **2005**, *15*, 458.
(47) Schlichte, K.; Kratzke, T.; Kaskel, S. *Microporous Mesoporous Mater.* **2004**, *73*, 81.